Structural Engineering and Mechanics, *Vol. 69, No. 6 (2019) 667-676*
DOI: https://doi.org/10.12989/sem.2019.69.6.667

Ant lion optimizer for optimization of finite perforated metallic plate

Mohammad H. Bayati Chaleshtari[a] and Mohammad Jafari*

Faculty of Mechanical and Mechatronics Engineering, Shahrood University of Technology, Shahrood, Iran

(Received August 31, 2017, Revised January 31, 2019, Accepted February 5, 2019)

Abstract. Minimizing the stress concentration around hypotrochoid hole in finite metallic plates under in-plane loading is an important consideration in engineering design. In the analysis of finite metallic plate, the effective factors on stress distribution around holes include curvature radius of the corner of the hole, hole orientation, plate's aspect ratio, and hole size. This paper aims to investigate the impact of these factors on stress analysis of finite metallic plate with central hypotrochoid hole. To obtain the lowest value of stress around a hypotrochoid hole, a swarm intelligence optimization method named ant lion optimizer is used. In this study, with the hypothesis of plane stress circumstances, analytical solution of Muskhelishvili's complex variable method and conformal mapping is employed. The plate is taken into account to be finite, isotropic and linearly elastic. By applying suitable boundary conditions and least square boundary collocation technique, undefined coefficients of stress function are found. The results revealed that by choosing the above-mentioned factor correctly, the lowest value of stress would be obtained around the hole allowing to an increment in load-bearing capacity of the structure.

Keywords: finite metallic plates; stress concentration factor; hypotrochoid hole; analytical solution; ant lion optimizer

1. Introduction

Many types of research have paid attention to stress distribution around holes in a perforated plate and different methods were utilized. The complex variable method is one of the most useful techniques for solving a problem. (Motok 1997) studied the effect of bluntness on stress distribution around various holes in the infinite plate under axial loading.

(Louhghalam *et al.* 2011) showed how the complex variable approach can be numerically coupled with the finite element method to analyze stress distribution in plates with rectangular holes; in this case, cracks (Banh and Lee 2018) may be also common to treat stress concentration. (Batista 2011) investigated stress distribution around polygonal cutouts with complex geometries and Schwarz-Christoffel mapping function. (Banerjee *et al.* 2013) studied stress distribution around circular cutout on isotropic and orthotropic plates under transverse loading using a numerical method.

Meta-heuristic optimization methods have gained significant attention in various engineering applications since they have simple conceptions and cool to implement, without any gradient info, may evade local optimum and may be used in an extensive range of issues. Thus, numerous scientists have endeavored to employ them into various issues in different fields including Ant Colony Optimization (ACO), artificial bee colony (ABC), Genetic Algorithm (GA) (Dashti *et al.* 2018), Simulated Annealing (SA) (Rezakazemi *et al.* 2011), Particle Swarm Optimization (PSO) (Rezakazemi *et al.* 2017, Dashti *et al.* 2018), and etc. to the design of composite structures. Based on complex variable method, (Jafari *et al.* 2018) used an analytical method to optimize the symmetrical composite laminates with non-circular cutouts and failure strength of infinite orthotropic plates by means of GA. To find the minimum of stress around a quasi-triangular cutout, the Dragonfly Algorithm (DA) technique was used by (Jafari and Bayati Chaleshtari 2017). They achieved the best conditions of factor influencing the minimum normalized stress around the quasi-triangular cutout. Rotation angle, load angle, bluntness, fiber angle, and the material of the plate were considered as the design variables. Moreover, (Jafari and Bayati Chaleshtari 2017) used gray wolf optimization algorithm (GWO) to investigated the impact of various factors on the stress of infinite orthotropic plates with central polygonal cutout. The curvature radius of the corner of the cutout, load angle, cutout orientation and fiber angle for orthotropic materials was considered as the effective factors on stress distribution around cutouts.

Ant Lion Optimizer (ALO) has been recently used as a bio-inspired algorithm. This algorithm mimics the manners of ant lion hunting ants in nature. As a comparison with GA, PSO, and Cuckoo System (CS), this method is designed by some equations and engineering problems to reveal that ALO has better performance in convergence, local optima prevention, and robustness. (Nischal and Shivani 2015) presented the ALO technique to formulate the optimal load dispatch issue. He compared the results of ALO for three, six and twenty generating unit systems with other techniques. (Yao and Wang 2017) proposed a dynamic adaptive ALO for route planning of unmanned aerial vehicle. (Petrović *et al.* 2015) optimized combinatorial NP-hard flexible process planning problem

*Corresponding author, Associate Professor
E-mail: m_jafari821@shahroodut.ac.ir
[a]E-mail: mhbayati88@gmail.com

http://www.techno-press.com/journals/sem&subpage=7 ISSN: 1225-4568 (Print), 1598-6217 (Online)

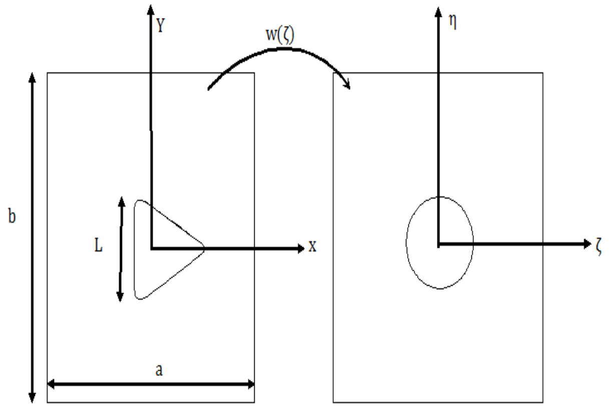

Fig. 1 A schematic of the plate with a triangular hole converting to a circular hole

and the performance of the ALO algorithm was compared with GA, SA, and PSO. The results indicated that the proposed algorithm performs better than other bio-inspired optimization algorithms. (Nischal and Mehta 2015) used the ALO to solve optimal load dispatch problem for three, six and twenty generating unit systems. (Mouassa *et al.* 2017) used a developed algorithm inspired by the hunting mechanism of antlions in nature for solving optimal reactive power dispatch (ORPD) problem.

The main aim of this study is to exhibit that the ALO is an algorithm with appropriate performance in optimizing the finite plates with different hole shapes. Also, in this research, according to the analytical solution based on complex variable and conformal mapping, the effect of important parameters on stress analysis of a finite metallic plate with various holes is investigated when the plate is subjected to in-plane loading (shear load uniaxial tensile, and biaxial). ALO is also used to optimize the effective parameters such as curvature radius of the corner of the cutout, the rotation angle of the hole, the ratio of plate's sides and the ratio of hole size to plate size.

2. Theoretical methods

The main goal of this paper is to optimize the stress and effective factors on the stress distribution of metallic finite plate with regular polygon hole in the linear elastic region. In such plate, the proportion of hole domain to the lengthiest domain is higher than 0.2. The problem is assessed according to the hypothesis of the in-plane stress without volumetric forces. The hole is presumed to be situated at the midpoint and far from external loads ($\sigma_\rho=\sigma_{\rho\theta}=0$). The rotation angle of the hole that signifies its location based on the horizontal is indicated by β.

The plate is under biaxial, uniaxial and shear loadings. The goal is to evaluate the impacts of various factors such as the hole corner radius of curvature, the shape of the hole, ratio of hole size to plate size, the rotation angle of the hole (β), and the type of in-plane loading on the optimum SCF. It must be pointed out that in this paper λ=0 and 2 are taken for uniaxial and biaxial loadings, respectively. To analyze the stress of non-circular holes, first, the problem of the plate with a dissimilar hole in complex plane z must be transformed into to problem of the plate with a circular hole with unit radius in the mapping plane ζ. This is performed using Eq. (1) where R (R=1), n, and m are diameter, hole type, corner curvature, respectively. Fig. 1 displays this transformation for triangular hole.

$\forall n$, $m=0$	$n=2$ $m>0$	$n=3$ $m>0$	$n=4$ $m>0$	$n=5$ $m>0$	$n=6$ $m>0$	$n=7$ $m>0$

Fig. 2 Effect of n on the creation of a hole

$$z = x + iy = w(\zeta) = R(\zeta + \frac{m}{\zeta^n}) \tag{1}$$

where $m\geq 0$ is a measure of sharpness or curvature of the corner. Varying m for a certain hole results in a different radius of curvature, and the resulting stress in different directions should be investigated. For m=0, the hole is a circle while increasing m rounds the hole.

The impact of n on the formation of various holes is presented in Fig. 2. As observed, the number of domains of the hole is n+1.

The complex variable ζ in ρ and θ coordinate is as Eq. (2)

$$\zeta = \rho e^{i\theta} = \rho(\cos\theta + i\sin\theta) \tag{2}$$

By considering Eqs. (3)-(4)

$$e^{in\theta} = \cos(n\theta) + i\sin(n\theta) \tag{3}$$

$$e^{-in\theta} = \cos(n\theta) - i\sin(n\theta) \tag{4}$$

By replacing the above equation in Eq. (1) and separating the imaginary and real parts, x and y coordinates are yielded.

$$x = \mathrm{Re}[w(\zeta)] = R(\rho\cos(\theta) + \frac{m\cos(n\theta)}{\rho^n}) \tag{5}$$

$$y = \mathrm{Im}\,g[w(\zeta)] = R(\rho\sin(\theta) + \frac{m\sin(n\theta)}{\rho^n}) \tag{6}$$

The modeling is assessed according to the complex variable method and plane elasticity theory. In the absence of volumetric forces, the compatibility equation in terms of stress function U is as Eq. (7)

$$\frac{\partial^4 U}{\partial x^4} + 2\frac{\partial^4 U}{\partial x^2 \partial y^2} + \frac{\partial^4 U}{\partial y^4} = 0 \tag{7}$$

A solution of plane problems in elasticity theory is summarized in form of determination of bi-harmonic function $U(x,y)$. To this end, (Muskhelishvili 1966) recommended the below solution for Eq. (7)

$$U(x,y) = \mathrm{Re}[\bar{z}\varphi(z) + \theta(z)] \tag{8}$$

In Eq. (8), *Re* represents the real part of a complex expression. $\varphi(z)$ and $\theta(z)$ are analytical functions of complex variable z. Then, two holomorphic analytical functions $\varphi(z)$ and $\psi(z)=\theta'(z)$ were considered which satisfy boundary conditions on the external contour. By means of the conformal mapping, the stress components as a function of ξ are well-defined as below

$$\sigma_\rho + \sigma_\theta = \sigma_x + \sigma_y = 4\,\mathrm{Re}\left[\frac{\varphi'(\zeta)}{\omega'(\zeta)}\right] \tag{9}$$

$$\sigma_\theta - \sigma_\rho + 2i\tau_{\rho\theta} = (\sigma_y - \sigma_x + 2i\tau_{xy})e^{2i\alpha} = \frac{2\zeta^2}{\rho^2\overline{\omega'(\zeta)}}(\overline{\omega(\zeta)}\Phi'(\zeta) + \omega'(\zeta)\Psi(\zeta)) \tag{10}$$

where

$$e^{2i\alpha} = \frac{\zeta^2\omega'(\zeta)}{\rho^2\overline{\omega'(\zeta)}} \quad , \quad \Phi(\zeta) = \frac{\varphi'(\zeta)}{\omega'(\zeta)} \tag{11}$$

$$\Psi(\zeta) = \frac{\psi'(\zeta)}{\omega'(\zeta)} \quad , \quad \Phi'(\zeta) = \varphi''(\zeta)\omega'(\zeta)$$

Therefore

$$\sigma_\rho = \mathrm{Re}\left[\frac{2\varphi'(\zeta)}{\omega'(\zeta)} - \frac{\zeta^2}{\rho^2\overline{\omega'(\zeta)}}(\overline{\omega(\zeta)}\varphi''(\zeta)\omega'(\zeta) + \psi'(\zeta))\right] \tag{12}$$

$$\sigma_\theta = \mathrm{Re}\left[\frac{2\varphi'(\zeta)}{\omega'(\zeta)} + \frac{\zeta^2}{\rho^2\overline{\omega'(\zeta)}}(\overline{\omega(\zeta)}\varphi''(\zeta)\omega'(\zeta) + \psi'(\zeta))\right] \tag{13}$$

$$\tau_{\rho\theta} = \mathrm{Im}\,g\left[\frac{\zeta^2}{\rho^2\overline{\omega'(\zeta)}}(\overline{\omega(\zeta)}\varphi''(\zeta)\omega'(\zeta) + \psi'(\zeta))\right] \tag{14}$$

After calculating $\varphi(\xi)$ and $\psi(\xi)$ as well as substituting them in Eqs. (12)-(14), the stress components were obtained (Pan *et al.* 2013)

$$\varphi(\zeta) = \sum_{n=1}^{\infty} A_n\zeta^{-n} + \sum_{n=0}^{\infty} B_n\zeta^n \tag{15}$$

$$\psi(\zeta) = \sum_{n=1}^{\infty} \frac{C_n\zeta^{-n}}{\omega'(\zeta)} + \sum_{n=0}^{\infty} D_n\zeta^n \tag{16}$$

where A_n, B_n, C_n and D_n are complex numbers.

At the present, based on the above-mentioned equations, it is essential to estimate the unidentified coefficients remaining in Eqs. (15) and (16) to investigate the stress distribution around the hole. Hence, a least square boundary collocation approach is employed. To estimate the unidentified coefficients in Eq. (15), equidistance collocation points are chosen on the internal boundary in ζ-plane and on the external boundary in z-plane (Jafari and Ardalani 2016). Afterward, corresponding points related to the internal and external boundaries of the regular hole in z-plane and the finite plate in ζ-plane can be calculated by Eq. (1).

3. Ant lion optimizer (ALO)

Over the last decades, there has been a growing interest in algorithms inspired by the behaviors of natural phenomena (Dashti *et al.* 2018, Rezakazemi *et al.* 2018). It is shown by many researchers that these algorithms are well suited to solve complex computational problems. In this paper, ALO is used as a new optimization algorithm based on the lifecycle of ant lions in natural. This method mimics the hunting mechanism of ant lions in nature (Mirjalili 2015).

3.1 Inspiration

Ant lions are related to the Myrmeleontidae class and Neuroptera order. The lifecycle of ant lions involves two steps: larvae and adult. The first one is commonly recognized as “doodlebug” due to the trails it leaves in the sand whereas seeking for an excellent position to form its trap. Afterward, the ant lion hides on the bottom of pit and waits for insects particularly ants to be trapped. When an ant falls into the trap, it is hard to escape, as the ant lion throws sands out of pit with its mandible to force the victim to slide towards the bottom. Eventaully, the ant is dragged into the sand and eaten. Then, the ant lion amends the trap and waits for the next hunt. Besides, it should be pointed out that the size of pit is positively related to the strength of ant lions. Commonly, the more ants the ant lion has consumed, the stronger the ant lion, the bigger the pit size, the larger the probability of catching more ants. The modeling of the behavior of ant lions and ants is given in the following section by (Mirjalili 2015).

3.2 Mathematical model of ALO

To model ALO, ants are needed to travel across the seek space, and ant lions are permitted to hunt them and become fitter by traps. As ants travel stochastically in nature when seeking for food, a random walk is selected for modeling ants’ movement (Mirjalili 2015).

$$X(t) = [0, cumsum(2r(t_1)-1), cumsum(2r(t_2)-1), ..., cumsum(2r(t_n)-1)] \tag{17}$$

where *cumsum* calculates the cumulative sum, n is the maximum number of iteration, t exhibits the stage of random walk and $r(t)$ is a stochastic function calculated as Eq. (18)

$$r(t) = \begin{cases} 1 & if \quad rand > 0.5 \\ 0 & if \quad rand \le 0.5 \end{cases} \tag{18}$$

where t exhibits the stage of random walk and rand is a random number produced with homogenous distribution in the range of [0,1]. The positions of ants are preserved in a M_{Ant} matrix

$$M_{Ant} = \begin{bmatrix} A_{1,1} & A_{1,2} & \dots & A_{1,n} \\ A_{2,1} & A_{2,2} & \dots & A_{2,d} \\ \vdots & \vdots & \ddots & \vdots \\ A_{n,1} & A_{n,2} & \cdots & A_{n,d} \end{bmatrix} \tag{19}$$

where $A_{i,j}$ exhibits the value of the *j-th* variable of *i-th* ant, *n* is the number of ants, and *d* is the number of variables. Fitness function of each ant is preserved in the matrix M_{OA}

$$M_{OA} = \begin{bmatrix} f([A_{1,1}, A_{1,2}, \dots, A_{1,d}]) \\ f([A_{2,1}, A_{2,2}, \dots, A_{2,d}]) \\ \vdots \\ f([A_{n,1}, A_{n,2}, \dots, A_{n,d}]) \end{bmatrix} \tag{20}$$

where *f* is the objective function. In Eq. (19), $M_{Antlion}$ is the matrix for preserving the position of each ant lion, $AL_{i,j}$ exhibits the *j-th* dimension's value of *i-th* ant lion.

$$M_{Antlion} = \begin{bmatrix} AL_{1,1} & AL_{1,2} & \dots & AL_{1,n} \\ AL_{2,1} & AL_{2,2} & \dots & AL_{2,d} \\ \vdots & \vdots & \ddots & \vdots \\ AL_{n,1} & AL_{n,2} & \cdots & AL_{n,d} \end{bmatrix} \tag{21}$$

Analogously, the fitness function of each ant lion is preserved in the matrix M_{OAL}

$$M_{OAL} = \begin{bmatrix} f([AL_{1,1}, AL_{1,2}, \dots, AL_{1,d}]) \\ f([AL_{2,1}, AL_{2,2}, \dots, AL_{2,d}]) \\ \vdots \\ f([AL_{n,1}, AL_{n,2}, \dots, AL_{n,d}]) \end{bmatrix} \tag{22}$$

To keep the random walks inside the seek space; they are normalized using the Eq. (23)

$$X_i^t = \frac{(X_i^t - a_i) \times (b_i - c_i^t)}{(d_i^t - a_i)} + c_i \tag{23}$$

where a_i and b_i are the minimum and maximum of the random walk of *i-th* variable, respectively. c_i^t and d_i^t are the minimum and maximum of *i-th* variable at *t-th* iteration, respectively. The modeling of ants trapping in ant lion's pits is represented by the Eqs. (24)-(25)

$$c_i^t = Antlion_j^t + c^t \tag{24}$$

$$d_i^t = Antlion_j^t + d^t \tag{25}$$

where $Antlion_j^t$ exhibits the location of the *j-th* ant lion at *t-th* iteration. To model the ant lions's hunting capability, a roulette wheel is used.

Ant lions shoot sands outwards the center of the pit when they understand that an ant is in the trap. This slides down the trapped ant which is trying to escape. To model such action, the radius of ants' random walks hyper-sphere is reduced adaptively. Eqs. (26)-(27) are proposed in this regard by (Mirjalili 2015).

$$c^t = \frac{c^t}{I} \tag{26}$$

$$d^t = \frac{d^t}{I}$$

where I is a ratio calculated as Eq. (28)

$$I = 10^w . \frac{t}{T} \tag{28}$$

Where t is the current iteration, T is the maximum number of iterations, w is the constant that depends on current iteration as Eq. (29)

$$w = \begin{cases} 2 & if \quad t > 0.1T \\ 3 & if \quad t > 0.5T \\ 4 & if \quad t > 0.75T \\ 5 & if \quad t > 0.9T \\ 6 & if \quad t > 0.95T \end{cases} \tag{29}$$

Afterward, an ant lion is needed to renew its location to the latest location of the hunted ant to increase its chance of catching new prey (Mirjalili 2015)

$$Antlion_j^t = Ant_i^t \quad if \quad f(Ant_i^t) > f \tag{30}$$

where t exhibits the current iteration, $Antlion_j^t$ refers the location of chosen *j-th* ant lion at *t-th* iteration, and Ant_i^t illustrates the location of *i-th* ant at *t-th* iteration. The final section is elitism. It is presumed that each ant randomly walks around a selected ant lion by the roulette wheel (R_A^t) and the elite simultaneously (R_E^t) at *t-th* iteration as Eq. (31)

$$Ant_i^t = \frac{R_A^t + R_E^t}{2} \tag{31}$$

where Ant_i^t indicates the location of *i-th* ant at *t-th* iteration.

4. Verification of results

For verification of the ALO results, two well-known algorithms i.e., PSO and GA algorithms are chosen. To gather measurable findings, all algorithms are implemented on the test functions several times and statistical test is used to consider outcomes and confirms that the outcomes are statistically noteworthy. In this study, the Wilcoxon test with α<0.05 and two assumptions is also performed. The null assumption denotes to the performance equality of the three optimization algorithms ($H_0: \chi_1 = \chi_2 = \chi_3$), and other assumption is one hypothesis which denotes to the nonappearance of equality that algorithms and confirms the advantage of ALO compared to GA and PSO algorithms

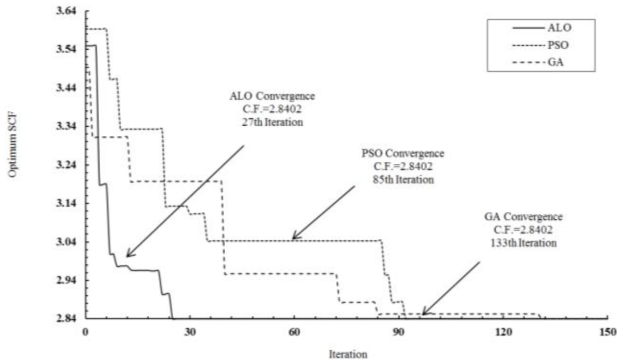

Fig. 3 Comparing convergence diagram of ALO, PSO and GA

Table 1 Material properties of the plate

Material	E (GPa)	ν
Steel	207	0.3

$(H_1: \chi_1 \neq \chi_2 \neq \chi_3)$. Based on findings achieved from the Wilcoxon test, the P values found by this method is between the ALO and GA (0.043). Also, the P value of this method is between the ALO and PSO (0.045). The P values indicate that this superiority is statistically substantial as their values are below 0.05. Consequently, the first assumption is excluded. The ALO algorithm profits from high exploitation which helps the ALO algorithm to quickly converge to the global optimum and exploit it precisely.

The convergence diagram for steel plate with a square hole in one of the optimum conditions m=0.03218, β=9.4257, L/a=0.2 and under bi-axial loading is shown in Fig. 3. The constraints, comprise of lower and upper boundaries, can be altered upon the hole shape. The results prove that in the iterations of 150, the best convergence can be attained for ALO in 27 iterations, while for GA and PSO algorithms converges after 133 and 85 iterations, respectively. As observed, the ALO converges quicker than both GA and PSO and the optimum findings achieved by ALO are further better. Using CPU 2.66GHz, convergence times for ALO, PSO, GA was 71, 105 and 155 s respectively, which confirms that the ALO in less time to achieve the suitable convergence.

5. Results

The mechanical properties of the plate used in this study are given in Table 1. According to the fact that in isotropic materials, the type of material does not affect stress concentration, only results associated with steel are presented. Here, the optimum values of normalized stress in metallic finite plates with square, triangular, hexagonal and pentagonal holes under biaxial, uniaxial and shear loadings are presented. The various factors including the shape of the hole, the rotation angle of the hole and bluntness and ratio of hole size to the plate are taken into account. In this study, finite metallic plates with hypotrochoid holes are considered. Therefore, it is first tried to examine the optimum values of design parameters and a minimum value of SCF of the hole in each ratio of hole size to plate size, using ALO algorithm.

5.1 Triangular hole

Table 2 exhibits the impact of the hole size ratio to plate on the value of cost function by simultaneous consideration of rotation angle and cutout radius of curvature as design variables and compare optimal stress values obtained by solving an infinite plate (L/a=0.01) for metallic finite plate with triangular hole subjected to in-plane loadings (b/a=1). In this section, the optimization is performed for three design variables i.e., ratio of hole size to plate size, hole corner radius of curvature and rotation angle to find the optimum value of normalized stress in terms of the optimum rotation angle and hole curvature. It is clarified in Table 2, with increasing the ratio of L/a, the value of optimum SCF increases in three type of loading. It is obvious that for the L/a ratio less than 0.2, enhancing the ratio have not a remarkable impact on the changes of stress concentration and the percentage error is less than 10%. Then, infinite plate solution can be applied for these ratios. Whereas for ratios higher than 0.2, by enhancing L/a, the value of stress concentration enhances significantly and the percentage difference for the examination of optimum SCF of the perforated finite plate by the theory of infinite plates reaches 129.43% in L/a=0.6. This clearly shows that effective of the ratio of hole size to plate size in a finite plate. Moreover, for m=0 (circular hole), the cost function of all loading states is minimum. Fig. 4 exhibits the impact of hole size to plate size ratio on the value of optimum SCF for finite metallic plate subjected to in-plane loadings. Furthermore, Fig. 5 shows the maximum optimum stress in terms of L/a in the three aforementioned loadings states. As observed, by increasing the ratio of hole size to plate size in the range of L/a less than 0.2 the value of optimum stress is approximately constant. Furthermore, in the range of L/a greater than 0.2 the values of optimum stress increase with increasing L/a. Moreover, the impact of L/a is more noticeable for uniaxial loading than other types of loading, therefore the rate of increase in the optimum SCF is more severe in this type of loading.

5.2 Square hole

For the square hole, the optimum values of effective parameters, optimum SCF and the comparison of optimum stress values obtained by solving an infinite plate (L/a=0.01) with a metallic finite plate subjected to in-plane loadings (b/a=1) are presented in Table 3. The optimum values of rotation angle, hole corner radius of curvature and normalized stress are the outputs of the ALO. The findings in Table 3 indicate that the value of SCF less than circular hole can be achieved by choosing suitable values for the effective parameters such as rotation angle. Also, Table 3 shows that with increasing L/a, the values of optimum stress concentration increase in all three types of loading. For the L/a ratios less than 0.2, the percentage difference is below 20% for all types of loading. While for ratios higher than 0.2, the value of stress concentration enhances significantly and the percentage difference for the examination of

Table 2 Optimum results for triangular hole in various values of L/a (b/a=1)

L/a	Uni-axial loading		Bi-axial loading		Shear loading	
	Optimum SCF	Percentage Difference	Optimum SCF	Percentage Difference	Optimum SCF	Percentage Difference
0.01	3.0006	0	2.8871	0	2.3099	0
0.1	3.0643	2.12	2.9316	1.54	2.365	2.38
0.2	3.266	8.84	3.0708	6.36	2.5386	9.9
0.3	3.6354	21.15	3.3207	15.02	2.8502	23.4
0.4	4.24	41.30	3.7193	28.82	3.3322	44.25
0.5	5.2214	74.01	4.3485	50.61	4.0244	74.22
0.6	6.8843	129.43	5.3859	86.55	4.9504	114.31

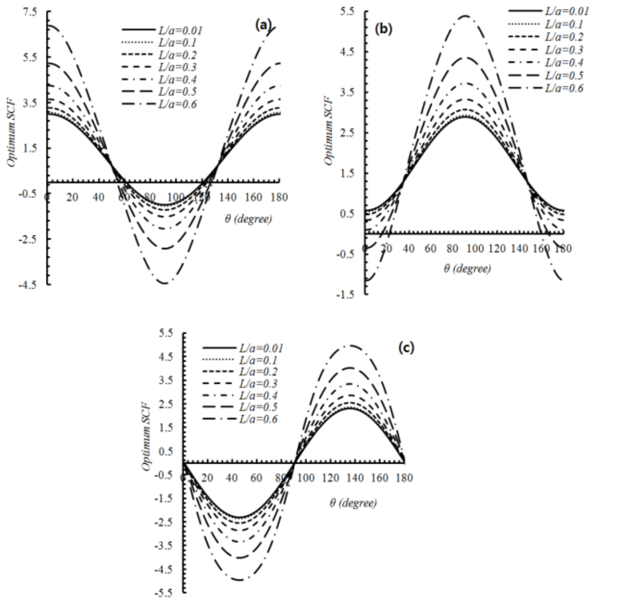

Fig. 4 Optimum SCF in a finite plate with a triangular hole under (a) uni-axial (b) bi-axial and (c) shear loadings for different values of *L*/*a*

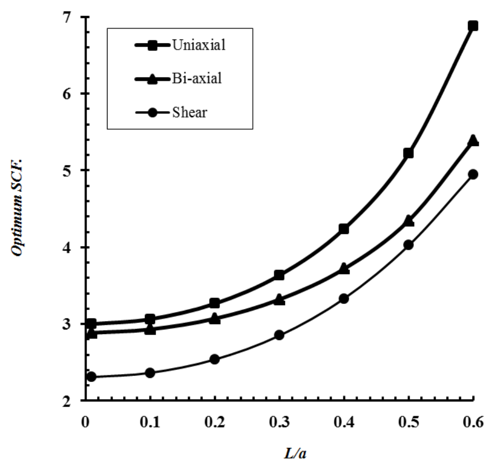

Fig. 5 Maximum optimum SCF with *L*/*a* for triangular hole in different loading

optimum SCF of the perforated finite plate by the theory of infinite plates reaches 304% in some cases. Therefore, we cannot use of the infinite plate solution for these ratios. In

Table 3 Optimum results for square hole in various values of L/a (b/a = 1)

Type of Loading	*L*/*a*	β	*m*	Optimum SCF	Percentage Difference
Uni-axial	0.01	47.1252	0.05625	2.4709	0
	0.1	21.9899	0.05857	2.5594	3.58
	0.2	22.9902	0.06431	2.8497	15.33
	0.3	28.274	0.06446	3.4057	37.83
	0.4	28.2712	0.06630	4.2529	72.11
	0.5	9.4252	0.08847	5.3684	117.26
	0.6	53.4103	0.09332	6.7285	172.30
Bi-axial	0.01	9.4196	0.02846	2.5652	0
	0.1	53.4066	0.02921	2.6728	4.19
	0.2	9.4257	0.03218	2.8402	10.72
	0.3	21.9918	0.03565	3.25	26.69
	0.4	47.1208	0.03985	3.994	55.69
	0.5	21.9905	0.05117	5.4707	113.26
	0.6	21.991	0.07086	10.3663	304.11
Shear	0.01	3.5549	0.08953	1.7739	0
	0.1	41.7267	0.08938	1.8460	4.06
	0.2	4.6238	0.09325	2.0797	17.23
	0.3	1.1847	0.09278	2.5294	42.58
	0.4	38.7713	0.09566	3.2914	85.54
	0.5	11.4861	0.09538	4.1634	134.70
	0.6	53.268	0.09702	4.6447	161.83

addition to Fig. 6 exhibits the stress distribution around the hole after applying the optimum values of mentioned effective parameters in three types of loading for different ratio of hole size to plate size.

Fig. 7 exhibits the maximum optimum stress concentration in various *L*/*a* ratios for biaxial, uniaxial, and the shear loadings. In all loadings, with increasing *L*/*a*, optimum SCF increases. The effect of *L*/*a* is more pronounced for biaxial loading.

5.3 Pentagonal cutout

Optimum stress values obtained from various ratios of hole size to plate size for a finite metallic plate with a pentagonal hole is presented in Table 4. According to this table, with increasing *L*/*a*, the optimum SCF in all three types of loadings increases. Also, for the ratios of *L*/*a* greater than 0.2, by changing *L*/*a*, the optimum SCF rises significantly but for the ratio of *L*/*a* less than 0.2, increasing the ratio do not have a significant effect on variation of SCF. Moreover, in the pentagonal hole, m = 0 that represents a circular hole and yields the minimum value of cost function for all types of loading. Fig. 8 exhibits the stress distribution around the hole after applying optimum values for the aforementioned effective parameters in the three types of loading and different ratios of hole size to plate size. As observed, as *L*/*a* increases, in all three types of loading, the optimum values of SCF stress increase. Furthermore, Fig. 9 shows the variation of maximum

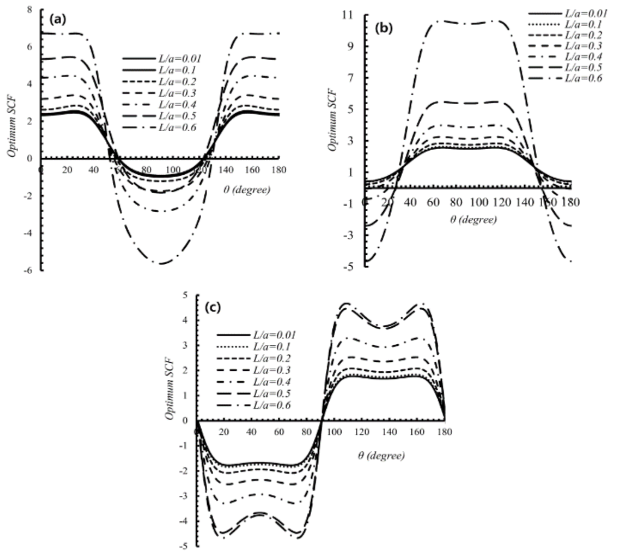

Fig. 6 Optimum SCF in a finite plate with a square hole under (a) uni-axial (b) bi-axial and (c) shear loadings for different values of *L*/*a*

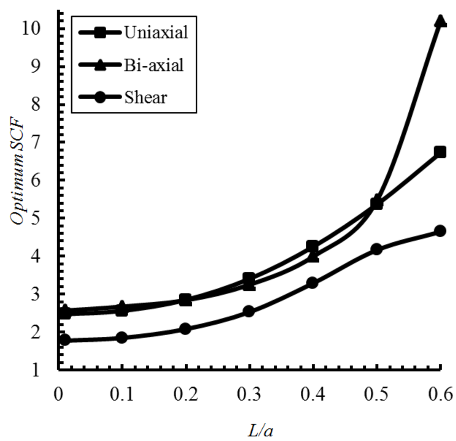

Fig. 7 Maximum optimum SCF with *L*/*a* for square hole in different loadings

optimum SCF in terms of *L*/*a* in the three mentioned loadings. Similar to the triangular hole for all ratio of *L*/*a*, by increasing the ratio of hole size to plate size in the range of less than 0.2 the value of optimum stress is approximately constant. Then, the solution is satisfactory for these ratios.

Moreover, in the range of greater than 0.2 the values of optimum stress increase and the percentage difference reaches 182.26% for uni-axial loading in *L*/*a*=0.6. As observed, increasing rate of SCF for the uniaxial loading is quicker than another loading.

5.4 Hexagonal hole

The difference of optimum SCF of a finite plate with a hexagonal hole as function of bluntness and rotation angle for various ratios *L*/*a* is presented in Table 5. The results indicate that for different ratios of *L*/*a*, the hexagonal hole ($m\neq0$) leads to the optimum SCF less than those of circular hole (m=0). This will be possible by proper selection of the

Table 4 Optimum results for pentagonal hole in various values of L/a (b/a = 1)

	Uni-axial loading		Bi-axial loading		Shear loading	
L/*a*	Optimum SCF	Percentage Difference	Optimum SCF	Percentage Difference	Optimum SCF	Percentage Difference
0.01	3.0008	0	2.8872	0	2.31	0
0.1	3.078	2.57	2.9411	1.86	2.3767	2.88
0.2	3.3248	10.79	3.1109	7.74	2.5888	12.06
0.3	3.7871	26.20	3.4217	18.51	2.9747	28.77
0.4	4.5744	52.43	3.9357	36.31	3.5810	55.02
0.5	5.9351	97.78	4.7972	66.15	4.4577	92.97
0.6	8.4702	182.26	6.3557	120.13	5.5908	142.02

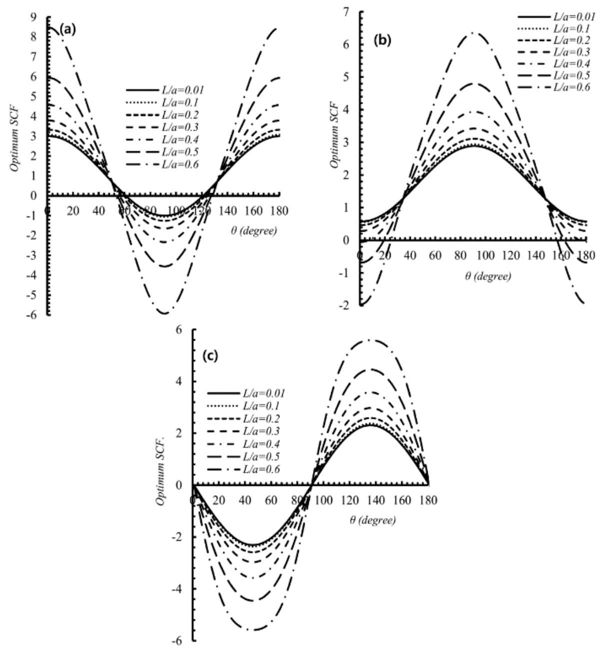

Fig. 8 Optimum SCF in a finite plate with a pentagonal hole under (a) uni-axial (b) bi-axial and (c) shear loadings for different values of *L*/*a*

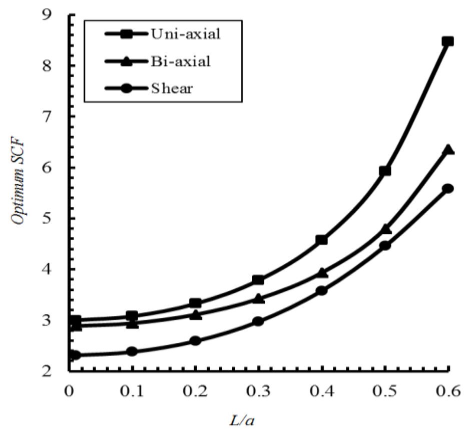

Fig. 9 Maximum optimum SCF with *L*/*a* for a pentagonal hole in different loadings

effective parameters values. Also, for the ratio of *L*/*a* less than 0.2, the percentage difference between the results obtained by finite and infinite plate solutions is less than

Table 5 Optimum results for hexagonal hole in different values of L/a (b/a = 1)

Type of Loading	*L*/*a*	*β*	*m*	Optimum SCF	Percentage Difference
Uni-axial	0.01	29.6935	0.01374	2.7398	0
	0.1	21.9887	0.01340	2.8083	2.5
	0.2	65.9809	0.01513	3.0299	10.58
	0.3	15.7076	0.01470	3.4344	25.35
	0.4	15.7053	0.01581	4.1217	50.43
	0.5	21.989	0.01838	5.2688	92.30
	0.6	53.4093	0.02381	7.2862	165.93
Bi-axial	0.01	0	0.00764	2.7341	0
	0.1	0	0.00776	2.7828	1.78
	0.2	0	0.00811	2.9370	7.42
	0.3	0	0.00862	3.2204	17.78
	0.4	0	0.00942	3.6858	34.80
	0.5	0	0.01087	4.4465	62.63
	0.6	0	0.01376	5.7526	110.40
Shear	0.01	29.8407	0.02314	2.0154	0
	0.1	10.9956	0.02356	2.0737	2.89
	0.2	73.8262	0.02293	2.2594	12.10
	0.3	10.9965	0.02257	2.6002	29.01
	0.4	23.5703	0.02082	3.1562	56.60
	0.5	54.9795	0.01863	3.9985	98.39
	0.6	17.2805	0.01416	5.2311	159.55

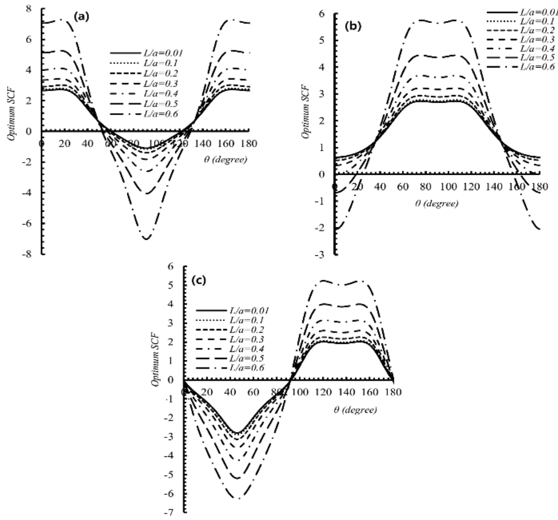

Fig. 10 Optimum SCF in a finite plate with a hexagonal hole under (a) uni-axial, (b) bi-axial and (c) shear loadings for different values of *L*/*a*

20%. While for higher ratios, the percentage difference for the assessment of optimum SCF of the perforated a finite plate by the theory of infinite plates is 165.93% for uni-axial loading in *L*/*a*=0.6. Moreover, Fig. 9 exhibits the stress distribution around the hole after applying the optimum values of the mentioned effective factors in three different loadings and ratios of hole size to plate size.

Fig. 11 shows maximum optimum SCF in terms of *L*/*a* in the three aforementioned loadings. As it is clear, the optimum SCF enhances by an increment the ratio of *L*/*a*. Furthermore, the effectiveness of the ratio of hole size to plate size on uni-axial loading is greater than others loadings.

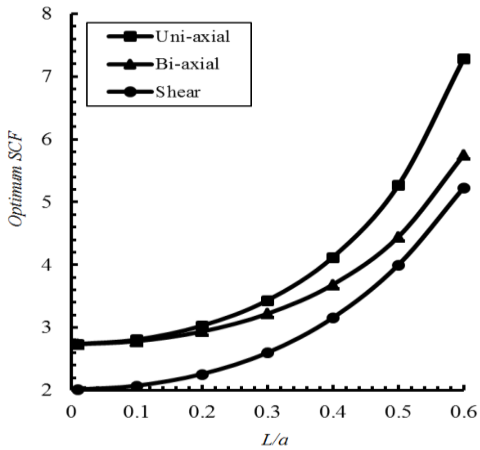

Fig. 11 Maximum optimum SCF with *L*/*a* for a hexagonal hole in different loadings

6. Scope of application of infinite plate theory

In this section, for different cutouts and bluntness parameters, different ratios of *L*/*a* that the percentage difference between the results obtained by finite and infinite plate theory is less than 10% are listed in Table 6. In fact, this table indicates that what aspect ratio (*L*/*a*) for different holes leads to the percentage difference of less than 10% when we use infinite plate theory. For various holes the aspect ratio is different. Also, with enhancing the value of bluntness parameter (*m*), the ratio of *L*/*a* increases.

7. Conclusions

In the current work, the ability of the ALO algorithm to optimize the finite perforated plates was examined. The optimal values of factors influencing the stress distribution around hypotrochoid hole located in the center of the finite metallic plate at different ratios of hole size to plate under in-plane loading were determined. Design variables in this study were the curvature of hole corners, the rotation angle of the hole, the aspect ratio of the plate, the ratio of hole size to plate size and the type of loading. In this study, the cost function was taken into account to be the value of SCF obtained based on the Muskhelishvili complex variable and conformal mapping with plane stress assumption. The stress functions in the finite plate with hypotrochoid hole were calculated by superposition of the stress function in the infinite plate having a hypotrochoid hole with stress function in the finite plate free of hole. The unidentified coefficients were determined using least squares boundary approach and proper boundary conditions. The optimum value of bluntness parameter (*m*) for all holes with an odd number of sides was *m*=0 which is equal to a circular hole.

Table 6 Scope of application of infinite plate theory for different holes

Type of Loading	L/a	β	Optimum SCF	Percentage Difference
Triangular Hole				
m=0.1				
Uni-axial	0.21	102.098	3.7522	9.35
Bi-axial	0.26	0	3.924	9.9
Shear	0.2	123.117	2.7499	9.87
m=0.2				
Type of Loading	L/a	β	Optimum SCF	Percentage Difference
Uni-axial	0.22	120.95	5.0902	9.63
Bi-axial	0.26	0	5.682	9.2
Shear	0.2	58.9195	3.418	9.8
m=0.3				
Type of Loading	L/a	β	Optimum SCF	Percentage Difference
Uni-axial	0.22	98.9596	7.9896	9.8
Bi-axial	0.27	0	9.39	9.5
Shear	0.2	27.4895	4.93	9.87
Square Hole				
m=0.05				
Type of Loading	L/a	β	Optimum SCF	Percentage Difference
Uni-axial	0.16	40.8443	2.714	9.7
Bi-axial	0.2	15.6988	2.9421	9.4
Shear	0.15	0	2.1006	9.8
m=0.1				
Type of Loading	L/a	β	Optimum SCF	Percentage Difference
Uni-axial	0.17	40.8378	2.9779	9.2
Bi-axial	0.22	40.8422	3.7637	9.2
Shear	0.15	0	1.946	9.3
m=0. 15				
Type of Loading	L/a	β	Optimum SCF	Percentage Difference
Uni-axial	0.19	40.8403	3.818	9.7
Bi-axial	0.24	40.8408	5.240	9.9
Shear	0.15	0	2.153	9.1
Pentagonal Hole				
m=0.05				
Type of Loading	L/a	β	Optimum SCF	Percentage Difference
Uni-axial	0.19	136.6591	4.2233	9.3
Bi-axial	0.23	0	4.3142	9.7
Shear	0.18	139.0151	3.076	9.7
m=0.8				
Type of Loading	L/a	β	Optimum SCF	Percentage Difference
Uni-axial	0.19	98.9569	5.2914	9.2
Bi-axial	0.23	0	5.4878	9.5
Shear	0.18	19.6351	3.7616	9.8
m=0.12				
Type of Loading	L/a	β	Optimum SCF	Percentage Difference

Table 6 Continued

Uni-axial	0.19	139.8018	7.5646	9.18
Bi-axial	0.23	0	7.9282	9.43
Shear	0.18	44.7674	5.2591	9.9
Hexagonal Hole				
m=0.05				
Type of Loading	L/a	β	Optimum SCF	Percentage Difference
Uni-axial	0.2	78.5393	3.7679	9.56
Bi-axial	0.25	0	4.234	9.9
Shear	0.18	80.1079	2.461	9.7
m=0.08				
Type of Loading	L/a	β	Optimum SCF	Percentage Difference
Uni-axial	0.2	9.4247	5.0619	9.1
Bi-axial	0.25	0	5.84	9.8
Shear	0.18	17.2795	3.123	9.9
m=0.12				
Type of Loading	L/a	β	Optimum SCF	Percentage Difference
Uni-axial	0.2	53.4073	8.4961	9.1
Bi-axial	0.25	0	9.85	9.3
Shear	0.18	86.3941	4.9969	9.9

While, for the holes with an even number of sides, the optimum conditions happened when $m\neq0$. For these holes, by choosing appropriate values for the effective parameters, SCF less than circular holes could be achieved. Moreover, results showed that for particular L/a values the determination of stress distribution in finite plates by means of infinite plates theory can allow to remarkable differences. These ratios for different holes and bluntness were presented. Results obtained from ALO showed an excellent balance between exploitation and exploration which leads to high local optimum avoidance and an appropriate convergence. Therefore, it can be found that ALO is a reliable and appropriate technique for optimizing a finite metallic plate.

References

Banerjee, M., Jain, N.K. and Sanyal, S. (2013), “Stress concentration in isotropic & orthotropic composite plates with center circular hole subjected to transverse static loading”, *Int. J. Mech. Industr. Eng.*, **3**(1), 109-113.

Banh, T.T. and Lee, D. (2018), “Multi-material topology optimization design for continuum structures with crack patterns”, *Compos. Struct.*, **186**, 193-209.

Batista, M. (2011), “On the stress concentration around a hole in an infinite plate subject to a uniform load at infinity”, *Int. J. Mech. Sci.*, **53**(4), 254-261.

Dashti, A., Asghari, M., Dehghani, M., Rezakazemi, M., Mohammadi, A.H. and Bhatia, S.K. (2018), “Molecular dynamics, grand canonical Monte Carlo and expert simulations and modeling of water-acetic acid pervaporation using polyvinyl alcohol/tetraethyl orthosilicates membrane”, *J. Molecul. Liq.*, **265**, 53-68.

Dashti, A., Asghari, M., Solymani, H., Rezakazemi, M. and Akbari, A. (2018), "Modeling of $CaCl_2$ removal by positively charged polysulfone-based nanofiltration membrane using artificial neural network and genetic programming", *Desalinat. Water Treat.*, **111**, 57-67.

Dashti, A., Harami, H.R. and Rezakazemi, M. (2018), "Accurate prediction of solubility of gases within H2-selective nanocomposite membranes using committee machine intelligent system", *Int. J. Hydrog. Energy*, **43**(13), 6614-6624.

Dashti, A., Riasat Harami, H., Rezakazemi, M. and Shirazian, S. (2018), "Estimating CH4 and CO_2 solubilities in ionic liquids using computational intelligence approaches", *J. Molecul. Liq.*, **271**, 661-669.

Jafari, M. and Ardalani, E. (2016), "Stress concentration in finite metallic plates with regular holes", *Int. J. Mech. Sci.*, **106**, 220-230.

Jafari, M. and Bayati Chaleshtari, M.H. (2017), "Optimum design of effective parameters for orthotropic plates with polygonal cut-out", *Lat. Am. J. Sol. Struct.*, **14**, 906-929.

Jafari, M. and Bayati Chaleshtari, M.H. (2017), "Using dragonfly algorithm for optimization of orthotropic infinite plates with a quasi-triangular cut-out", *Eur. J. Mech.-A/Sol.*, **66**, 1-14.

Jafari, M., Moussavian, H. and Chaleshtari, M.H.B.J.S. (2018), "Optimum design of perforated orthotropic and laminated composite plates under in-plane loading by genetic algorithm", *Struct. Multidiscipl. Optim.*, **57**(1), 341-357.

Louhghalam, A., Igusa, T., Park, C., Choi, S. and Kim, K. (2011), "Analysis of stress concentrations in plates with rectangular openings by a combined conformal mapping-finite element approach", *Int. J. Sol. Struct.*, **48**(13), 1991-2004.

Mirjalili, S. (2015), "The ant lion optimizer", *Adv. Eng. Softw.*, **83**, 80-98.

Motok, M.D. (1997), "Stress concentration on the contour of a plate opening of an arbitrary corner radius of curvature", *Mar. Struct.*, **10**(1), 1-12.

Mouassa, S., Bouktir, T. and Salhi, A. (2017), "Ant lion optimizer for solving optimal reactive power dispatch problem in power systems", *Eng. Sci. Technol.*, **20**(3), 885-895.

Muskhelishvili, N. (1966), *Some Basic Problems of the Mathematical Theory of Elasticity*, Nauka, Moscow, Russia.

Nischal, M.M. and Mehta, S. (2015), "Optimal load dispatch using ant lion optimization", *Int. J. Eng. Res. Appl.*, **5**(8), 10-19.

Nischal, M.M. and Shivani, M. (2015), "Optimal load dispatch using ant lion optimization", *Int. J. Eng. Res. Appl.*, **5**(8), 10-19.

Pan, Z., Cheng, Y. and Liu, J. (2013), "Stress analysis of a finite plate with a rectangular hole subjected to uniaxial tension using modified stress functions", *Int. J. Mech. Sci.*, **75**, 265-277.

Petrović, M., Petronijevic, J., Mitic, M. and Vuković, N. (2015), "The ant lion optimization algorithm for flexible process planning", *Product. Eng.*, **18**(2), 65-68.

Rezakazemi, M., Azarafza, A., Dashti, A. and Shirazian, S. (2018), "Development of hybrid models for prediction of gas permeation through FS/POSS/PDMS nanocomposite membranes", *Int. J. Hydrog. Energy*, **43**(36), 17283-17294.

Rezakazemi, M., Dashti, A., Asghari, M. and Shirazian, S. (2017), "H2-selective mixed matrix membranes modeling using ANFIS, PSO-ANFIS, GA-ANFIS", *Int. J. Hydrog. Energy*, **42**(22), 15211-15225.

Rezakazemi, M., Razavi, S., Mohammadi, T. and Nazari, A.G. (2011), "Simulation and determination of optimum conditions of pervaporative dehydration of isopropanol process using synthesized PVA-APTEOS/TEOS nanocomposite membranes by means of expert systems", *J. Membr. Sci.*, **379**(1), 224-232.

Yao, P. and Wang, H. (2017), "Dynamic adaptive ant lion optimizer applied to route planning for unmanned aerial vehicle", *Soft Comput.*, **21**(18), 5475-5488.

CC